arXiv:1112.5324v1 [hep-ph] 22 Dec 2011

DO-TH 11/28
ADP-11-42/T764

Probing Minimal Flavor Violation with Long–Lived Stops and Light Gravitinos at Hadron Colliders

J. S. Kim
Institut für Physik, Technische Universität Dortmund, D-44221 Dortmund, Germany
ARC Centre of Excellence for Particle Physics at the Terascale,
School of Chemistry and Physics, University of Adelaide, Adelaide, Australia

H. Sedello
Institut für Physik, Technische Universität Dortmund, D-44221 Dortmund, Germany

In the framework of minimal flavor violation (MFV), we discuss the decay properties of a supersymmetric scalar top (stop) in the presence of a light gravitino. Given a small mass difference between the lighter stop and lightest neutralino and an otherwise sufficiently decoupled spectrum, the stop may be long–lived and thus can provide support to MFV at hadron colliders. For a bino–like lightest neutralino, we apply bounds from searches in the $\gamma\gamma\not{E}_T$ channel (ATLAS with $1\,\mathrm{fb}^{-1}$ and DØ with $6.3\,\mathrm{fb}^{-1}$) and give a $5\,\mathrm{fb}^{-1}$ projection for the ATLAS search.

I. INTRODUCTION

Supersymmetry (SUSY) [1] is an attractive extension of the standard model (SM). However the simplest version of a supersymmetric SM, the minimal supersymmetric standard model (MSSM) [2], does not predict a specific flavor structure; all superrenormalizable soft supersymmetry breaking terms allowed by gauge and Lorentz symmetry as well as R parity are present in its Lagrange density [2]. However, it is clear that a supersymmetric extension of the standard model must have a non–generic flavor structure to be compatible with experimental results [3, 4].

The way the standard model flavor structure is extended to the MSSM is not unique, yet a widely discussed flavor scheme is minimal flavor violation [5] (MFV). In MFV the standard model Yukawa couplings are promoted to spurion fields transforming under the SM flavor group to restore the SM's flavor symmetry. If all additional flavor structure of a new physics model can be understood as higher dimensional flavor invariant operators including these spurions and the model's fields, the model is called MFV.

As the LHC is running and eventually will find supersymmetry, it will be challenging to investigate the flavor structure at a hadron collider due to the detectors' limited flavor identification abilities and the complexity of the recorded events. In [6] it was pointed out that the third generation's squarks decouple from the first two generations in MFV. As a result, a light stop can be long–lived decaying through the flavor changing neutral current channel [7, 8]

$$\tilde{t}_1 \to c\tilde{\chi}_1^0, \tag{1}$$

if all flavor diagonal channels are kinematically closed. ($\tilde{t}_1$ denotes the light stop, $\tilde{\chi}_1^0$ the lightest neutralino and c a charm quark.) An observation of long–living light stops thus would hint in the direction of MFV.

In MFV, the coupling Y between $\tilde{t}_1$, c and $\tilde{\chi}_1^0$ is

$$Y \propto \lambda_b^2 V_{cb} V_{tb}^*, \tag{2}$$

where λ_b and V_{ij} denotes the bottom Yukawa coupling and elements of the Cabibbo Kobayashi Maskawa (CKM) matrix respectively. The precise value of Y depends on the stop left–right composition, the neutralino decomposition, and on a numeric factor stemming from the MFV expansion; see Ref. [6] for details.

In [9] it is shown that the average transverse impact parameters for the stop decay products can be expected to be $\mathcal{O}(1800\,\mu\mathrm{m})$ for stop lifetimes of the order of ten ps in the production channel $pp \to \overline{t}\overline{t}\tilde{t}_1\tilde{t}_1$ [10] . When both top quarks in this channel decay leptonically, the pair of same signed leptons in the final state allows to separate the signal process from its SM background; however, the small leptonic branching ratio of top quarks suppresses this process so that, after applying all kinematic cuts, only few events are left in this channel. Ref. [11] proposes an alternative collider signature assuming stop pair production in association with one hard jet. Demanding a minimum transverse momentum of 1 TeV for the additional jet, the whole parameter region consistent with electroweak baryogenesis can be probed. Ref. [12] considers an analogous process, stop pair production in association with two b–jets. However, these two studies do not consider stops in the MFV framework.

If we consider local SUSY instead of a global implementation of SUSY, we can have distinct collider signal signatures with little SM background: In local SUSY, a massive gravitino emerges in the supersymmetric mass spectrum [13]. Its interactions with other particles are severely suppressed by the reduced Planck mass

$$m_{\mathrm{Pl}} = (8\pi G_N)^{-\frac{1}{2}} = 2.4 \times 10^{18}\,\mathrm{GeV}, \tag{3}$$

where G_N is Newton's constant. Depending on the exact breaking mechanism in the hidden sector, the gravitino can be very light. A light gravitino interacts through its goldstino components with couplings proportional to

$$(m_{3/2} m_{\mathrm{Pl}})^{-1}, \tag{4}$$

where $m_{3/2}$ is the gravitino mass.

In models of gauge mediation [14–18], $m_{3/2}$ is generally much smaller than the sparticle mass scale; thus, the gravitino is the lightest supersymmetric particle (LSP). Its goldstino interactions are enhanced and can be of the electroweak order.

Consequently, the lightest neutralino decays via

$$\tilde{\chi}_1^0 \to X\tilde{G}, \tag{5}$$

where X denotes a photon, Z, or a Higgs boson; $\tilde{G}$ denotes a gravitino [19]. If X is a photon (γ), this decay leads to very clear collider signatures with high p_T isolated photons plus missing transverse energy ($\not{E}_T$) stemming from gravitinos leaving the detector unseen.

Several studies with light gravitinos at hadron colliders were performed in the past. Ref. [19–21] consider the diphoton plus $\not{E}_T$ channel at hadron colliders. In Ref. [22, 23] the authors examine a stau NLSP and a gravitino LSP. A sneutrino NLSP and a gravitino LSP scenario is investigated in Ref. [24, 25]. Ref. [26] considers the discovery potential of a neutralino NLSP and a gravitino LSP at the Tevatron, where they consider a general decomposition of the lightest neutralino. In Ref. [19] the authors consider a light stop NNLSP and a light neutralino NLSP and a gravitino LSP. Ref. [27] investigate a stop NLSP and a gravitino LSP scenario for the Tevatron as well as the LHC. A chargino NLSP and a gravitino LSP is considered in Ref. [28]. Depending on the size of the gravitino mass, non–pointing photons can be measured. The discovery potential of sparticle decays with a finite decay length are investigated in [29–31]. A recent experimental search for sparticles with finite decay lengths is published in [32].

In this paper we investigate the parameter region where the decay in Eq. (1) is dominant in the context of a light gravitino, and how the stop masses are constrained in this framework by recent collider searches, assuming that $\tilde{t}_1$, $\tilde{\chi}_1^0$, and $\tilde{G}$ are the only light supersymmetric particles. We discuss the stop and $\tilde{\chi}_1^0$ decay patterns in section II. In section III we apply collider bounds in the $\gamma\gamma\not{E}_T$ channel [33, 34]. The cuts adapted from the experimental studies are discussed in the two appendices.

II. DECAY PATTERNS

A. Light stop decays

Here we discuss possible decay patterns of light stops and their implications on the parameter space. We start with decays of the light stop via Yukawa and gauge couplings and then discuss direct stop decays into a gravitino.

The lighter stop mass eigenstate $\tilde{t}_1$ is the lightest squark state in many supersymmetry breaking scenarios. On one hand, the large top Yukawa coupling can induce a sizable left-right mixing in the stop sector leading to light $\tilde{t}_1$ masses. On the other hand, if the soft squark mass terms are unified at a high scale, the stop mass terms are prominently reduced by the top Yukawa coupling in the running of the renormalization group equations to the electroweak scale [38]. In this case, $\tilde{t}_1$ is mostly a $SU(2)$ singlet state since its mass term does not receive any contributions from $SU(2)$ gaugino loops. In addition, right–handed stop loop contributions to the rho parameter are sufficiently suppressed [39].

Surprisingly light masses of $\mathcal{O}(100\,\mathrm{GeV})$ are still consistent with experimental searches for stops decaying to $c\tilde{\chi}_1^0$ at the Tevatron if the mass splitting

$$\Delta m = m_{\tilde{t}_1} - m_{\tilde{\chi}_1^0} \tag{6}$$

is smaller than $\approx 30\,\mathrm{GeV}$ [40].

Since we want the flavor changing decay in Eq. (1) to be the dominant decay and the stop to be long–lived, we must ensure that the potentially dominant decays $\tilde{t}_1 \to t\tilde{\chi}_1^0$, $\tilde{t}_1 \to b\tilde{\chi}_1^{\pm}$, and $\tilde{t}_1 \to b\tilde{\chi}_1^0 W$ are kinematically closed or sufficiently suppressed,

$$m_{\tilde{t}_1} < m_b + m_{\tilde{\chi}_1^0} + m_W, \quad m_{\tilde{t}_1} < m_b + m_{\tilde{\chi}_1^{\pm}}. \tag{7}$$

Depending on the chargino and slepton masses ($> m_{\tilde{t}_1}$), the four–body decay $\tilde{t}_1 \to b\ell\nu\tilde{\chi}_1^0$ may be dominant if Δm exceeds a few $10\,\mathrm{GeV}$. For small stop neutralino mass splittings, the tree–level four–body decay is strongly phase space suppressed and Eq. (1) remains the dominant decay mode [6].

The MFV decay width can be written as

$$\Gamma(\tilde{t}_1 \to c\tilde{\chi}_1^0) = \frac{m_{\tilde{t}_1} Y^2}{4\pi}\left(\frac{\Delta m}{m_{\tilde{t}_1}}\right)^2 \tag{8}$$

in the limit of $\Delta m \ll m_{\tilde{t}_1}$ [6]. Thus, if this decay is dominant, the stop lifetime is governed by $\Delta m Y$. The kinetic energy of the hadronic stop decay remnants depends on the size of the mass splitting Δm. In a study with same-sign leptons [9], a major reduction of event numbers due to a minimal p_T cut on these low energy decay products has been found.

In the presence of a light gravitino, restrictions on Δm and Y are not sufficient to guarantee the dominance of the FCNC (flavor changing neutral current) decay mode Eq. (1). If $\Delta m Y$ is too small, the two–body decays of the stop into the gravitino,

$$\tilde{t}_1 \to \tilde{G}c, \quad \tilde{t}_1 \to \tilde{G}t, \tag{9}$$

and—if the resonant decay to tops is kinematically closed—the three–body decay mode of the stop,

$$\tilde{t}_1 \to \tilde{G}bW, \tag{10}$$

can have a significant contribution to the full stop decay width. These decays can invalidate our assumption, that the stop dominantly decays via a FCNC process with a finite impact parameter.

For the flavor diagonal two and three–body decay channels, the decay rates are [19, 41]

$$\Gamma(\tilde{t}_1 \to t\tilde{G}) = \frac{1}{48\pi}\frac{m_{\tilde{t}_1}^5}{m_{\rm Pl}^2 m_{3/2}^2}\left(1-x_t^2\right)^4 \tag{11a}$$

$$\begin{aligned}\Gamma(\tilde{t}_1 \to W^+ b\tilde{G}) = &\frac{V_{tb}^2\alpha_{em}}{384\pi^2\sin^2\theta_W}\frac{m_{\tilde{t}_1}^5}{m_{\rm Pl}^2 m_{3/2}^2}\\ &\cdot\left[|c_L|^2\, I\left(x_W^2,x_t^2\right)+|c_R|^2 J\left(x_W^2,x_t^2\right)\right], \end{aligned}\tag{11b}$$

where the gravitino mass is neglected in the phase space integrals. α_{em}, and θ_W denote the fine-structure constant and the Weinberg angle, respectively. Further $x_W = m_W/m_{\tilde{t}_1}$ and $x_t = m_t/m_{\tilde{t}_1}$ with the top mass m_t. c_L and c_R parametrize the $\tilde{t}_L$ and $\tilde{t}_R$ contribution to $\tilde{t}_1$; due to the 3rd generation's decoupling in MFV the other squarks' admixture is small, *i.e.* $|c_L|^2 + |c_R|^2 \approx 1$. The functions $I(x_W^2, x_t^2)$ and $J(x_W^2, x_t^2)$ are phase space integrals and can be found in [41]. Note that Eq. (11b) does not comprise the finite top width and diverges at the top mass threshold. We use this formula for $m_{\tilde{t}_1} < m_t$ only. As the three–body decay proceeds trough a virtual top quark, its rate is largest for a right–handed stop, because the chirality flipping top mass dominates the propagator.

For a bino–like $\tilde{\chi}_1^0$, the flavor structure of the $\tilde{t}_1 - \tilde{G} - c$ coupling stemming from the MFV expansion is the same as in the $\tilde{t}_1 - \tilde{\chi}_1^0 - c$ coupling, thus the decay rate for $\tilde{t}_1 \to \tilde{G}c$ can be written as [9]

$$\Gamma(\tilde{t}_1 \to \tilde{G}c) = \frac{Y'^2}{48\pi}\frac{m_{\tilde{t}_1}^5}{m_{\rm Pl}^2 m_{3/2}^2}, \tag{12}$$

where Y' and Y are related by a factor dependent on the stop composition as Y comprises the hypercharges of the left- and right–handed stop fields. The factor is

$$\left|\frac{Y'}{Y}\right| = \frac{1}{\sqrt{2}g'Y_Q} \approx \begin{cases} 3 & \text{(right–handed } \tilde{t}_1) \\ 12 & \text{(left–handed } \tilde{t}_1) \end{cases} \tag{13}$$

with the SM $U(1)$ coupling g' and the left–handed (right–handed) stop hypercharge $Y_Q = \frac{1}{6}\left(\frac{2}{3}\right)$.

We show the branching ratio $\mathcal{B}(\tilde{t}_1 \to c\tilde{\chi}_1^0)$ and the stop lifetime in the $m_{\tilde{G}}$–Y plane for three different masses of a right–handed stop in Fig. 1 using the decay rates (8), (11), and (12). To generate the plots, we keep Δm fixed at 10 GeV and use $\sin^2\theta_W = 0.23$, $\alpha_{em} = 1/128$, and $m_t = 173$ GeV. The plot for left–handed stops does not differ significantly from the one shown.

Due to the $m_{\tilde{t}_1}^5$ dependence of the decay widths in Eqs (9), (10) and the weaker $m_{\tilde{t}_1}^{-1}$ dependence of $\Gamma(\tilde{t}_1 \to c\tilde{\chi}_1^0)$, the minimal gravitino mass necessary to account for a sizable $\mathcal{B}(\tilde{t}_1 \to c\tilde{\chi}_1^0)$ increases with larger stop masses. The $m_{\tilde{t}_1}^{-1}$ dependence of $\Gamma(\tilde{t}_1 \to c\tilde{\chi}_1^0)$ also causes the smallness of the shifts of the lifetime regions in Fig. 1 to larger Y values when the stop mass is increased.

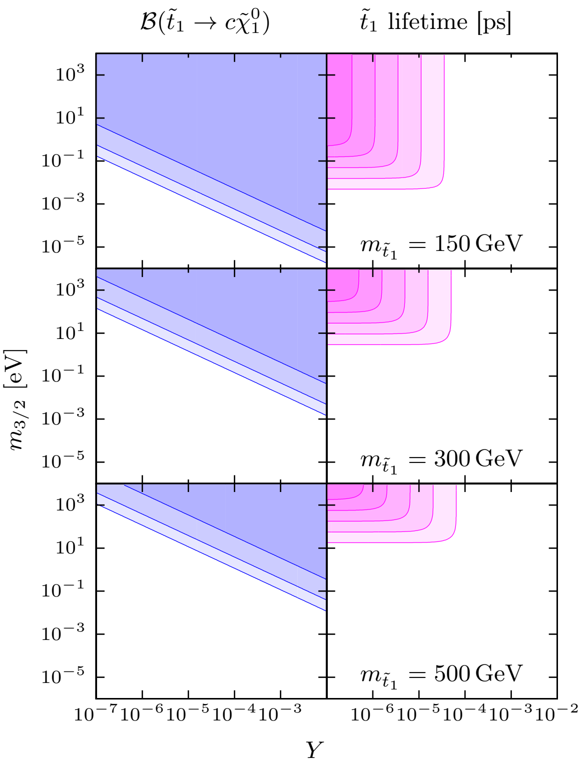

FIG. 1: MFV light stop branching ratios (left, blue) and stop lifetimes (right, pink), respectively for $m_{\tilde{t}_1} =$ 150 GeV, 300 GeV and 500 GeV (from top to bottom), in dependence on the gravitino mass $m_{\tilde{G}}$ and the MFV coupling Y. In the branching ratio plots, the shaded areas correspond to $\mathcal{B}(\tilde{t}_1 \to c\tilde{\chi}_1^0) \geq 0.01$, 0.1, 0.9 (from light to dark hue), whereas, in the lifetime plots, the shaded areas correspond to $\tau_{\tilde{t}_1} \geq 0.01$, 0.1, 1, 10, 100 ps (from light to dark hue). We chose $\Delta m = 10$ GeV.

As it is clearly visible from Fig. 1, very small values of $Y \lesssim \mathcal{O}(10^{-5})$ and at least gravitino masses of $\mathcal{O}(0.1 - 1\,\text{keV})$ are required in addition to the mass hierarchy

$$m_{3/2} \ll m_{\tilde{\chi}_1^0} \leq m_{\tilde{t}_1} \leq m_{\tilde{\chi}_1^\pm} \tag{14}$$

for the stop to be long–lived and to decay dominantly to $c\tilde{\chi}_1^0$.

As the charmed hadron produced in the decay has a macroscopic lifetime of $\mathcal{O}(1\,\text{ps})$ itself, however, a macroscopic stop lifetime might turn out to be accessible experimentally only if it exceeds this timescale.

B. NLSP neutralino composition and decays

Neutralinos are mass eigenstates of the $U(1)$ gauge fermion (bino), the neutral $SU(2)$ gauge fermion (wino), and the neutral up– and down–type Higgs fermion (higgsino). The fields' individual contributions to $\tilde{\chi}_1^0$ as well as the neutralino mass spectrum depends on the bino mass M_1, the wino mass M_2, the Higgs mixing parameter μ and the ratio between the up–type and down–type Higgs vacuum expectation value (VEV) $\tan\beta$. If $\tilde{\chi}_1^0$ is the NLSP and $\tilde{G}$ the LSP, $\tilde{\chi}_1^0$ decays via $\tilde{\chi}_1^0 \to X\tilde{G}$, where X is either the photon, the Z boson, or a neutral Higgs boson. Branching ratios into the various decay channels are fixed by phase space suppression factors and the decomposition of the lightest neutralino. General formulae for the decay widths are given in Refs [19, 26].

In the previous subsection, we argued that the mass of the light chargino $\tilde{\chi}_1^\pm$, a mass eigenstate of charged winos and higgsinos, has to be larger than the light stop mass in order to suppress the flavor diagonal stop decay to $\tilde{\chi}_1^\pm b$. This requirement cannot be satisfied if the $\tilde{\chi}_1^0$ is wino–like, *i.e.* if $M_2 \ll M_1, |\mu|$, as in this case both the $\tilde{\chi}_1^0$ and the $\tilde{\chi}_1^\pm$ mass are $\approx M_2$. The mass splitting between wino–like $\tilde{\chi}_1^\pm$ and $\tilde{\chi}_1^0$ is of the order of $\frac{m_Z^5}{\mu^4}$ [42], given $M_1 \ll |\mu|$, and thus is extremely suppressed for $|\mu| \gtrsim$ few 100 GeV.

Similarly, if $\tilde{\chi}_1^0$ is higgsino–like, $\tilde{\chi}_1^0$ and $\tilde{\chi}_1^\pm$ have masses of the same order of magnitude given by μ. The mass splitting $\Delta m_{\tilde{\chi}_1^\pm \tilde{\chi}_1^0}$ is of the order of $\frac{m_Z^2}{M_2}$ [42] for $|\mu| \ll M_1, M_2$.

If $\tilde{\chi}_1^0$ is bino–like, its mass is M_1 approximately, while the $\tilde{\chi}_1^\pm$ mass is given by $|\mu|$ or M_2. As the mass gap depends on two different supersymmetric mass parameters, it can be sizable depending on the details of high scale physics.

While in a mass region close to the Z mass, also a higgsino–like $\tilde{\chi}_1^0$ may respect the anticipated mass hierarchy in Eq. (14), we focus on a bino–like $\tilde{\chi}_1^0$ in discussing experimental bounds as 1) in the bino case the mass hierarchy can exist over a large stop mass scale and 2) binos have a large branching fraction to photons. For $m_{\tilde{\chi}_1^0} > m_Z$ and negligible phase space suppression, the branching ratio is $\mathcal{B}(\tilde{\chi}_1^0 \to \gamma\tilde{G}) \approx \cos^2\theta_W$. This value is obvious as $\tilde{G}$ is a gauge singlet and γ a mixed state of the hypercharge gauge boson and the neutral $SU(2)$ gauge boson where the mixture is parametrized by the Weinberg angle. Including the phase space suppression from m_Z and assuming that the higgsino sector is decoupled, the bino decay rates are [19, 43]

$$\Gamma(\tilde{\chi}_1^0 \to \gamma\tilde{G}) = \cos^2\theta_W \frac{m_{\tilde{\chi}_1^0}^5}{48\pi m_{3/2}^2 m_{\rm Pl}^2} \tag{15a}$$

$$\Gamma(\tilde{\chi}_1^0 \to Z\tilde{G}) = \sin^2\theta_W \frac{m_{\tilde{\chi}_1^0}^5}{48\pi m_{3/2}^2 m_{\rm Pl}^2} \left(1 - \frac{m_Z^2}{m_{\tilde{\chi}_1^0}^2}\right)^4 . \tag{15b}$$

For reference we show the bino–neutralino lifetime as a function of the lightest neutralino mass for gravitino masses 1, 10, 100, 1000 eV in Fig. 2.

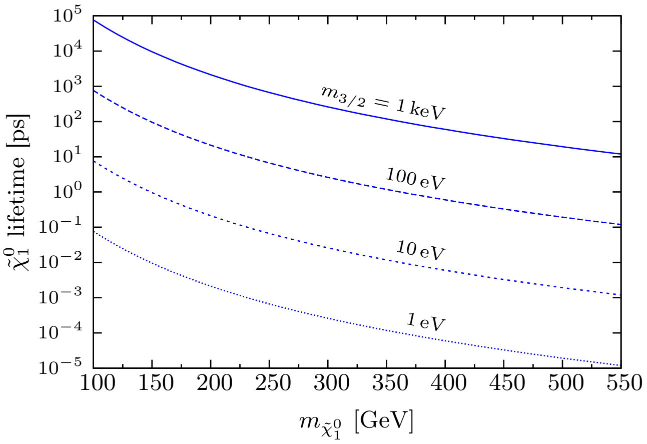

FIG. 2: Lightest neutralino lifetime as a function of the neutralino and gravitino mass.

III. COLLIDER BOUNDS

When $\tilde{t}_1$, $\tilde{\chi}_1^0$, and $\tilde{G}$ are the only light supersymmetric particles, stops are dominantly produced in pairs, both at $\bar{p}p$ and pp colliders,

$$\bar{p}p \to \tilde{t}_1\tilde{t}_1^*, \qquad pp \to \tilde{t}_1\tilde{t}_1^*. \tag{16}$$

The production cross sections are given in Fig. 3 as a function of the stop mass for the LHC at 7 TeV as well as for Tevatron and are calculated with `Prospino` [44] using the built-in CTEQ6.6M [45] parton distribution functions (PDFs). We also show the next–to–leading order uncertainty by varying the factorization scale (μ_F) and the renormalization scale (μ_R) between $\frac{1}{2}m_{\tilde{t}_1}$ and $2m_{\tilde{t}_1}$ while keeping μ_R equal to μ_F.

Given a bino–like $\tilde{\chi}_1^0$, the final state signatures of a decay chain via Eq. (1) and Eq. (5) are

$$\gamma\gamma c\bar{c}\tilde{G}\tilde{G}, \quad \gamma Z c\bar{c}\tilde{G}\tilde{G}, \quad ZZc\bar{c}\tilde{G}\tilde{G}. \tag{17}$$

In general, with a small mass gap Δm, the charm jets are too soft to be useful for event selection. Thus constrains on our parameter space can stem from searches for an excess in the $\gamma\gamma\not{E}_T$, $\gamma Z\not{E}_T$ and $ZZ\not{E}_T$ channels. As binos dominantly decay to $\gamma\tilde{G}$, the SM background is negligible for energetic photons, and large $\not{E}_T$ and high p_T photons are efficiently identified in multipurpose detectors, we concentrate on the $\gamma\gamma\not{E}_T$ channel in this work. Several experimental searches for the diphoton and $\not{E}_T$ channel have been published [33–37]. So far, no excess above the SM expectation has been found.

In the following, we present exclusion limits in the stop–gravitino mass plane derived from the latest ATLAS search in the $\gamma\gamma\not{E}_T$ channel for a luminosity ($\mathcal{L}$) of 1.07 fb^{-1} [34]. We derive also bounds from the D0 search with $\mathcal{L} = 6.3\,\mathrm{fb}^{-1}$ [33], and give a $\mathcal{L} = 5\,\mathrm{fb}^{-1}$ projection for the ATLAS bound.

The dominant SM background with $\not{E}_T$ originating from the hard process stems from $W + \gamma$, $W +$ jets,

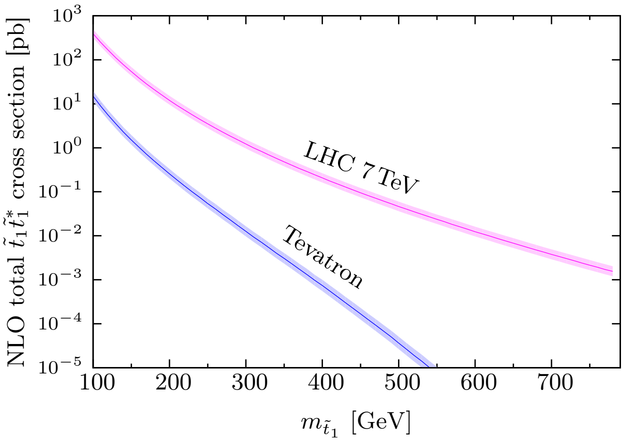

FIG. 3: NLO total cross section for $\tilde{t}_1\tilde{t}_1^*$ production at the Tevatron and at the LHC with $\sqrt{s} = 7\,\text{TeV}$. The colored bands correspond to scaling the unified scale $\mu_F = \mu_R = m_{\tilde{t}_1}$ by $\frac{1}{2}$ and 2.

and $W/Z\gamma(e)\gamma(e)$ production. Here, electrons/jets are misidentified as photons. SM background with $\not{E}_T$ from mismeasurements emerges from multijet production and direct photon production.

A supersymmetric background can only arise from $\tilde{\chi}_1^0\tilde{\chi}_1^0$ pair production as all other colored sparticles, sleptons, heavier neutralinos and charginos are assumed to be heavy and thus will have a negligible contribution. However, also the $\tilde{\chi}_1^0\tilde{\chi}_1^0$ production cross section is severely suppressed. In the limiting case of vanishing higgsino admixture to $\tilde{\chi}_1^0$, the cross section vanishes even at $\mathcal{O}(\alpha_{\text{EW}}^2\alpha_s)$. Consequently we do not take $\tilde{\chi}_1^0\tilde{\chi}_1^0$ pair production into account in the following.

A. Calculation of exclusion limits

To constrain the stop mass, the gravitino mass, and the MFV coupling Y, we calculate $\sigma_{\tilde{t}_1\tilde{t}_1^*}$, the total cross section for $\tilde{t}_1\tilde{t}_1^*$ production, in a grid of the light stop mass $m_{\tilde{t}_1}$ using `Prospino`. Note here that the light stop mass is the dominant SUSY parameter in the cross section [44], both for $p\bar{p}$ and pp initial states.

For each stop mass in the grid, we generate 100 000 $\tilde{t}_1\tilde{t}_1^*$ pair events with `pythia 6.4.25` [46] using the CTEQ6.6M [45] parton distribution functions. With the hadron level events we simulate the efficiency/acceptance for the $\gamma\gamma c\bar{c}\tilde{G}\tilde{G}$ final state in the ATLAS and DØ analyses employing a slightly modified version of `Delphes 1.9` [47][56]. The photon energy, and therefore our signal's detection efficiency, depends on the mass splitting Δm. As in the previous sections, we fix $\Delta m = 10\,\text{GeV}$. In appendices A and B, we give details on the cuts adopted from the experimental studies and on further simulation parameters. As a result of this simulation step, we obtain efficiencies ϵ_n in bins of $\not{E}_T$ and can calculate a signal cross section in bin n from

$$\sigma_n^{sig} = \epsilon_n \mathcal{B}(\tilde{t}_1 \to \tilde{\chi}_1^0 c)^2 \mathcal{B}(\tilde{\chi}_1^0 \to \tilde{G}\gamma)^2 \sigma_{\tilde{t}_1\tilde{t}_1^*}. \tag{18}$$

Using Eqs (15) to calculate $\mathcal{B}(\tilde{\chi}_1^0 \to \tilde{G}\gamma)$, we finally employ the CL$_s$ method [48, 49][57] to calculate the 95% exclusion limits for $\mathcal{B}(\tilde{t}_1 \to \tilde{\chi}_1^0 c)$. Those are depicted in Fig. 4, where we use the measurements plus background predictions of the experimental studies as enlisted in Tab. I. When calculating the exclusion limit, we treat the errors on the luminosity and the background as Gaussian nuisance parameters, see Tab. I, but do not take into account theory uncertainties stemming from scale variations and the choice of PDF sets.

The projection for the ATLAS study with a luminosity of $5\,\text{fb}^{-1}$ is calculated using the prescription of [50].

	$\not{E}_T$ Bin [GeV]	Observed events	SM bgd events
DØ [33]	$35 - 50$	18	11.9 ± 2.0
$(6.3 \pm 0.4)\,\text{fb}^{-1}$	$50 - 75$	3	5.0 ± 0.9
	> 75	1	1.9 ± 0.4
ATLAS [34]	> 125	5	4.1 ± 0.6
$(1.07 \pm 0.04)\,\text{fb}^{-1}$			

TABLE I: ATLAS and DØ measurements and background (bgd) predictions.

B. Numerical analysis and discussion

As can be seen in Fig. 4, the ATLAS search (solid pink curve) gives a bound on $\mathcal{B}(\tilde{t}_1 \to \tilde{\chi}_1^0 c)$ for stop masses up to 560 GeV. For a luminosity of $5\,\text{fb}^{-1}$, this mass is projected to 660 GeV. For larger masses, a dominant tree level FCNC decay $\tilde{t}_1 \to \tilde{\chi}_1^0 c$ is in agreement with the measurement. As can be seen from Fig. 4, the $1.07\,\text{fb}^{-1}$ ATLAS data already excludes a larger parameter region than the $6.3\,\text{fb}^{-1}$ DØ data [58].

For each stop mass, the bound in Fig. 4 can be mapped to a bound on the maximal gravitino mass for given values of Y using Eqs (8), (11), and (12). We plot these bounds for $Y = 10^{-7}$, 10^{-6}, 10^{-5} in Fig. 5. As Eqs (11) do not provide the correct stop width for masses in the threshold region close to the top mass, we exclude this region from the mapping and interpolate our result in the region $m_t \pm 30\,\text{GeV}$ ($m_t = 173\,\text{GeV}$).

The mass difference Δm enters the bounds in Fig. 5 through Eq. (8) and through the hardness of the photon p_T spectrum. For small changes in Δm, the latter dependency can be neglected, and the bounds depend on the product $(Y\Delta m)$ only. Therefore the bounds for other viable values of Δm can be derived from those shown for $\Delta m = 10\,\text{GeV}$ by rescaling Y.

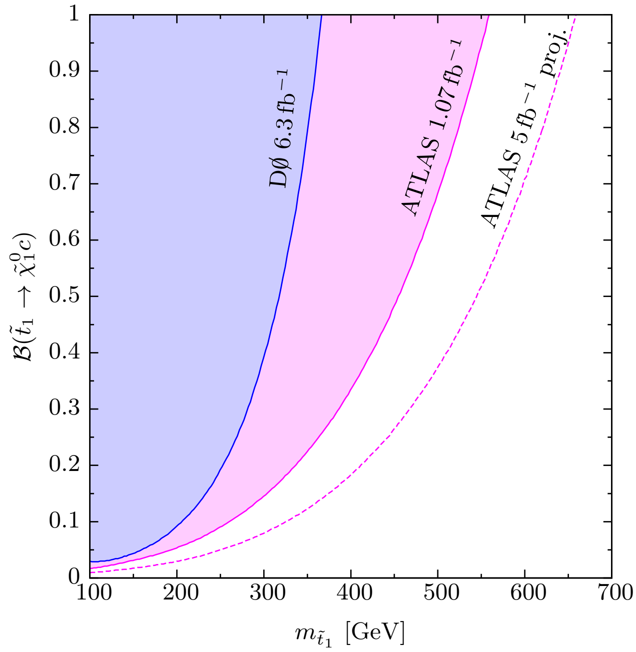

FIG. 4: Maximal branching ratio for $\tilde{t}_1 \to \tilde{\chi}_1^0 c$ in dependence of the stop mass given a bino-like $\tilde{\chi}_1^0$ and a fixed stop neutralino mass difference of $\Delta m = 10\,\text{GeV}$. Blue curve and blue shaded area: D∅ study [33]. Pink curves: ATLAS search [34], where the solid curve corresponds to the measurement, and the dashed line corresponds to a $\mathcal{L} = 5\,\text{fb}^{-1}$ projection. The areas above the curves are excluded at 95% CL within our simplified analysis.

Obviously, the smaller we choose Y the larger $m_{3/2}$ can be to generate a branching ratio below a certain value. The bound on $m_{3/2}$ resulting from the mapping in Fig. 5 varies over a wide mass range and thus potentially implies different regimes of $\tilde{t}_1$ and $\tilde{\chi}_1^0$ lifetimes; therefore, we show slopes of fixed values: For the $\tilde{\chi}_1^0$ lifetime, we show slopes for 1 fs, 1 ps, and 1 ns (black dotted) following approximately $m_{3/2} \propto m_{\tilde{t}_1}^{5/2}$. For $\tilde{t}_1$, we show slopes for 1/5 ps, 1 ps, and 5 ps (black solid). At $Y = 10^{-5}$, the stop lifetime is below 1 ps already induced by $\tilde{t}_1 \to \tilde{\chi}_1^0 c$ irrespective of the gravitational decay channels; therefore, only the 1/5 ps slope can be drawn here. Similarly, the stop lifetime drops below 1/5 ps for stop masses smaller than ≈ 230 GeV for $Y = 10^{-5}$, as $\Gamma(\tilde{t}_1 \to c\tilde{\chi}_1^0) \propto m_{\tilde{t}_1}^{-1}$ for fixed Δm. For both smaller values of Y, the stop lifetime slopes shown only depend weakly on Y because the corresponding total stop widths are dominated by the gravitational decay $\tilde{t}_1 \to t\tilde{G}$ resp. $\tilde{t}_1 \to W^+ b\tilde{G}$.

Fig. 5 shows that the gravitino mass region promoted in [9] as the region where the decay $\tilde{t}_1 \to \tilde{\chi}_1^0 c$ dominates for stop masses between 100 and 150 GeV is now disfavored. More generally, Fig. 5 allows to discuss two regimes of different orders of $\tilde{t}_1$ and $\tilde{\chi}_1^0$ lifetimes:

- In the stop mass region where $\mathcal{B}(\tilde{t}_1 \to \tilde{\chi}_1^0 c)$ is bounded, *i.e.* for $m_{\tilde{t}_1} \lesssim 500\,\text{GeV}$, the grav-

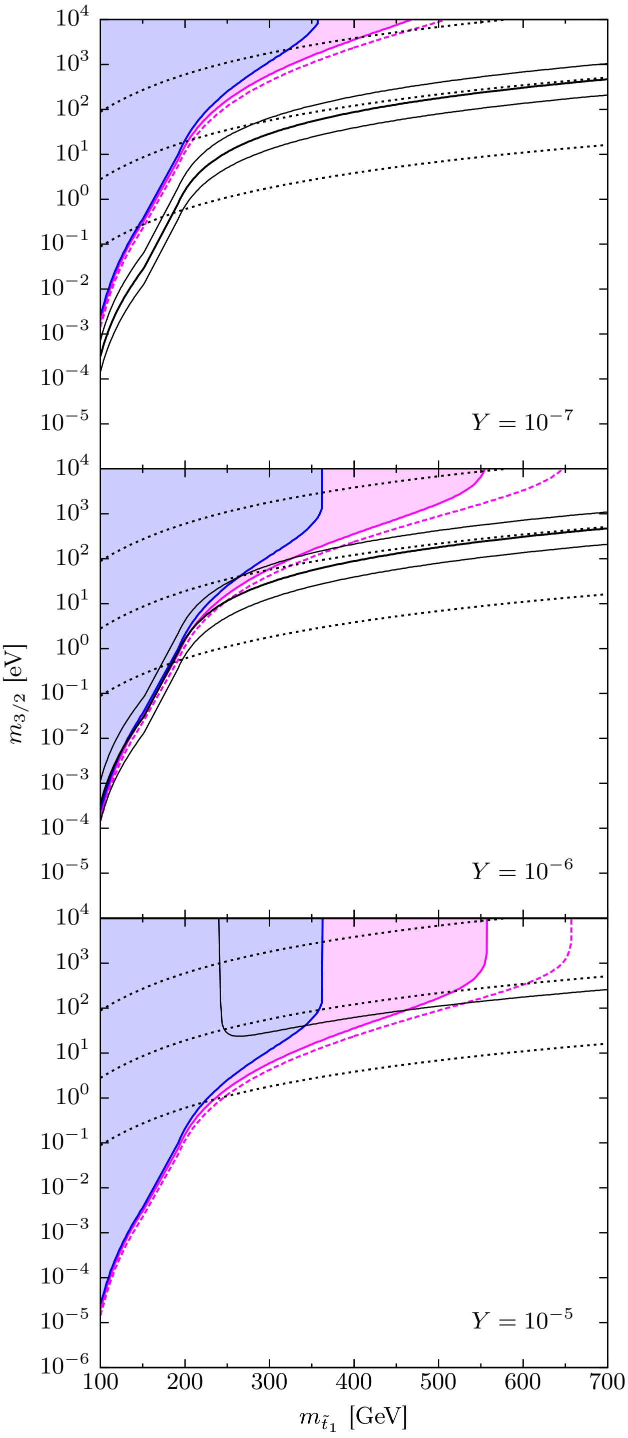

FIG. 5: Pink curves: The maximal gravitino mass respecting the ATLAS measurements [34] in dependence of the light stop's mass. The solid curve corresponds to the measurement for $\mathcal{L} = 1\,\text{fb}^{-1}$, and the dashed line corresponds to a $\mathcal{L} = 5\,\text{fb}^{-1}$ projection. Blue curve: $\mathcal{L} = 6.3\,\text{fb}^{-1}$ D∅ search [33]. Gravitino masses above the curves are excluded at 95% CL. The black dotted curves are slopes of fixed $\tilde{\chi}_1^0$ lifetime (1 fs, 1 ps, and 1 ns from bottom to top) for $m_{\tilde{\chi}_1^0} = m_{\tilde{t}_1} - 10\,\text{GeV}$. Along the solid black lines, the stop lifetime is 0.2 ps, 1 ps, and 5 ps.

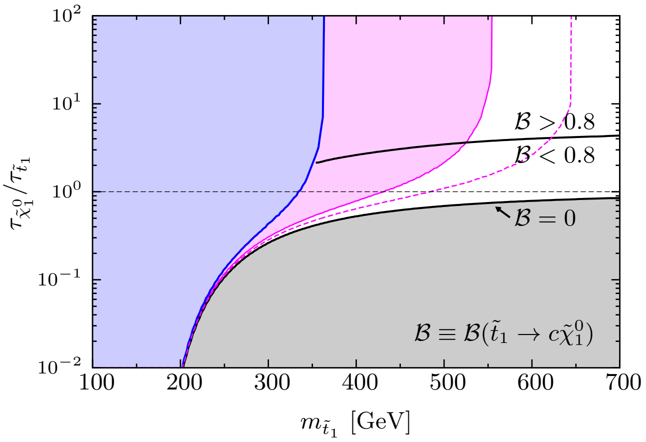

FIG. 6: White area: the available ratio of $\tilde{\chi}_1^0$ lifetime over $\tilde{t}_1$ lifetime for $Y = 10^{-6}$, $\Delta m = 10\,\text{GeV}$. Blue area: excluded by the DØ data [33]. Pink area: excluded by the $1.07\,\text{fb}^{-1}$ ATLAS data [34]. Pink dashed line: $5\,\text{fb}^{-1}$ projection for ATLAS. Grey area: invalid.

itino channels have a significant contribution to the stop decay. If this contribution is dominant, both—the $\tilde{\chi}_1^0$ and the $\tilde{t}_1$ decay—are governed by the same coupling $\sim 1/m_{3/2}^2$. As the stop decay width is suppressed by phase space ($t\tilde{G}$ channel) or top propagator ($\tilde{G}W^+b$ channel), the stop lifetime is expected to be larger than, or at the same order of magnitude as, the neutralino lifetime in this region.

- In the mass region where $\mathcal{B}(\tilde{t}_1 \to \tilde{\chi}_1^0 c)$ is allowed to dominate, *i.e.* for $m_{\tilde{t}_1} \gtrsim 500\,\text{GeV}$, the phase space suppression of the stop decay width Eq. (11a) is less pronounced; thus, the stop and neutralino gravitational partial decay widths are of the same order of magnitude. Consequently, if $\tilde{t}_1 \to c\tilde{\chi}_1^0$ is the dominant stop decay in this mass region, the stop lifetime is significantly smaller than the neutralino lifetime.

The relation between the stop and neutralino lifetimes ($\tau_{\tilde{t}_1}$ and $\tau_{\tilde{\chi}_1^0}$) described above is summarized in Fig. 6 where we plot the allowed ratio of both lifetimes within the bounds. Along the solid black line bounding the grey area, the contribution of Eq. (8) to the stop decay width vanishes; thus, this line represents the smallest value the ratio can have. The plot is generated for $Y = 10^{-6}$; however, only the leftmost parts of the exclusion areas depend weakly on the specific value of Y. For smaller masses, the bounds are driven by the phase space dependence of Eqs (11) and (15).

Note that for large $\tilde{t}_1$ or $\tilde{\chi}_1^0$ lifetimes, care must be taken in the interpretation of the bounds in Figs 5 and 6: The selection criteria for photon candidates in the ATLAS publication are chosen for prompt photons [51, 52]. Also, more explicitly, the DØ study requires that photon candidates point to a reconstructed primary vertex. We assumed in our calculation that all signal photons fulfill these criteria as if they were prompt. In a more realistic simulation, for increasing neutralino lifetimes, the signal photons' selection efficiency should decrease. For longitudinal neutralino decay lengths of $\mathcal{O}(1000\,\text{mm})$ ATLAS simulations show that for several photon selection criteria [59] used in [34] the efficiency drops from $\mathcal{O}(85\%)$ to $\mathcal{O}(55\%)$ [53]. Consequently, for lifetimes $\gtrsim \mathcal{O}(\text{ns})$, we overestimate the number of photons accepted, and the bounds on $m_{3/2}$ presented should be regarded with care in this lifetime region.

While for a bino–like neutralino, the $\gamma\gamma\not{E}_T$ channel offers the highest sensitivity for setting mass limits, it may be difficult to measure the neutralino lifetime in this channel due to lack of photon tracks. To construct the photons' impact parameters, CMS focuses on converted photons in a $2.1\,\text{fb}^{-1}$ search in the $\gamma\gamma\not{E}_T+$jets channel in [54]. As pointed out in [31], the $\tilde{\chi}_1^0 \to Z\tilde{G}$ channel may be used to investigate the neutralinos' lifetimes, as the Z's decay products allow to reconstruct the $\tilde{\chi}_1^0$'s trajectory.

IV. SUMMARY

In SUSY models with MFV, the third generation of squarks decouples from the other two generations. This decoupling opens the opportunity to support the MFV hypotheses with the measurement of a macroscopic stop decay length if the stop decay can only proceed through a generation–changing channel due to kinematic constraints [6]. In this work, we investigate the decay of a stop into a charm and a bino–like lightest neutralino with a subsequent bino decay to a photon and a light gravitino,

$$\tilde{t}_1 \to \tilde{\chi}_1^0(\to \gamma\tilde{G})c, \tag{19}$$

given a sufficiently small mass difference between $\tilde{t}_1$ and $\tilde{\chi}_1^0$.

While a macroscopic stop decay length serves as a hint for MFV, the neutralino's decay to a photon leaves a distinct signature in LHC and Tevatron detectors offering a good signal isolation.

Assuming that the remainder of the SUSY spectrum is decoupled, we find that the ATLAS search in the $\gamma\gamma\not{E}_T$ channel based on a luminosity of $1\,\text{fb}^{-1}$ [34] implies a bound on $\mathcal{B}(\tilde{t}_1 \to c\tilde{\chi}_1^0)$ for stop masses up to 560 GeV, see Fig. 4. In a $5\,\text{fb}^{-1}$ projection, the bound is raised to 660 GeV.

We find that stops lighter than $\sim 400\,\text{GeV}$ are still compatible with the $\gamma\gamma\not{E}_T$ searches; however, in this region, a significant fraction of the stops decays into gravitinos and quarks of the third generation. Here the stops are expected to have larger lifetimes than the lightest neutralinos; though, a macroscopic stop decay length is governed by the gravitino mass scale $m_{3/2}$ and is no hint for a decoupled stop flavor mixing structure.

Stops heavier than $\sim 500\,\text{GeV}$ can dominantly decay through the decay chain in Eq. (19) and eventually support MFV if they are a long–lived. As the lifetime depends on both the stops's flavor mixing and the gravitino mass, it can serve as a hint to MFV only if the contribution of the gravitino modes to the total decay width is negligible. This is assured if the neutralino lifetime is much larger than the stop lifetime.

We have discussed a split spectrum where the only light particles are a light gravitino, a light bino, and a light right–handed stop. It may be possible, however, to separate supersymmetric background processes in a scenario with additional light sparticles by vetoing on additional jets and/or isolated leptons.

Acknowledgments

We thank Manuel Drees, Sebastian Grab, and Gudrun Hiller for discussions in the initial phase of this project and for the comments on the manuscript. JSK also thanks the Bethe Center of Theoretical Physics and the Physikalisches Institut at the University of Bonn for their hospitality. This work has been supported in part by the Initiative and Networking Fund of the Helmholtz Association, Contract No. HA-101 ("Physics at the Terascale") and by the ARC Centre of Excellence for Particle Physics at the Terascale.

Appendix A: DØ cuts

Irrespective of the very clear signal event structure, we employ the fast detector simulation `Delphes` as a framework to calculate the signal efficiency. For DØ we use a simplified calorimeter layout composed from cells of dimension $0.1 \times \frac{2\pi}{64}$ in $\eta \times \phi$ space covering $|\eta| \leq 4.2$ and $\phi \in [0, 2\pi[$ where η denotes pseudorapidity and ϕ the azimuthal angle.

Jets are constructed employing the iterative midpoint algorithm with $R = 0.5$.

We adopt the cuts of [33] by requiring

- at least two isolated photons with $p_T > 25\,\text{GeV}$ and $|\eta| < 1.1$,
- the azimuthal angle between $\vec{\not{E}}_T$ and the hardest jet, if existent, is < 2.5,
- the azimuthal angles between $\vec{\not{E}}_T$ and both photons are > 0.2,
- $\not{E}_T > 35\,\text{GeV}$.

Photons must have 95% of their energy deposited in the electromagnetic calorimeter. For a photon to be isolated, the calorimetric isolation variable I defined in [33] must fulfill $I < 0.1$ and the scalar sum of transverse momenta of the tracks in a distance of $0.05 < R < 0.4$ from the photon must be smaller than $2\,\text{GeV}$. Here is $R = \sqrt{\Delta\phi^2 + \Delta\eta^2}$, where $\Delta\phi$ is a track's azimuthal distance from the photon and $\Delta\eta$ is the corresponding distance in pseudorapidity.

Note that nearly all signal events fulfill the isolation criteria hinting that the hadronic stop decay products are well separated from the photon stemming from the subsequent neutralino decay. This is expected as the neutralino decay products γ and $\tilde{G}$ are massless and thus the photon can have a large p_T relative to the stop flight direction.

Also note that we assume that a primary vertex can be reconstructed, and that the photon trajectories point to this vertex. The latter assumption should be regarded with care when the neutralino lifetime is large.

Appendix B: ATLAS cuts

We use the default ATLAS detector layout implemented in `Delphes` and apply the following simplified cuts:

- At least two isolated photons exist with $p_T > 25\,\text{GeV}$ and $|\eta| < 1.81$, but outside the transition region $1.37 < |\eta| < 1.52$,
- $\not{E}_T > 125\,\text{GeV}$

The ATLAS study employs a tight photon selection criterion on photon candidates, where the efficiency to identify a true (prompt) photon is approximately 85% in the kinematic region considered [51, 52]. We mimic this selection criterion by removing photons from our Monte Carlo sample with a probability of 15%.

We consider a photon to be isolated if in a cone of width $R = 0.2$, the scalar E_T sum is less than $5\,\text{GeV}$. Here we sum the E_T of the `Delphes` calorimeter cells and exclude the cell the photon is mapped to.

As for the DØ case, nearly all signal photons fulfill the isolation requirement. For larger $\tilde{\chi}_1^0$ masses, the main reduction of signal event numbers stems from the 85% photon selection efficiency.

---

[1] S. Ferrara, J. Wess and B. Zumino, Phys. Lett. B **51** (1974) 239.

[2] H. E. Haber, Nucl. Phys. Proc. Suppl. **62** (1998) 469 [arXiv:hep-ph/9709450].

[3] F. Gabbiani, E. Gabrielli, A. Masiero and L. Silvestrini, Nucl. Phys. B **477** (1996) 321 [arXiv:hep-ph/9604387].

[4] C. Amsler *et al.* [Particle Data Group], Phys. Lett. B **667** (2008) 1.

[5] G. D'Ambrosio, G. F. Giudice, G. Isidori and A. Stru-

mia, Nucl. Phys. B **645** (2002) 155 [arXiv:hep-ph/0207036].

[6] G. Hiller and Y. Nir, JHEP **0803** (2008) 046 [arXiv:0802.0916 [hep-ph]].

[7] K. i. Hikasa and M. Kobayashi, Phys. Rev. D **36** (1987) 724.

[8] M. Muhlleitner and E. Popenda, JHEP **1104** (2011) 095 [arXiv:1102.5712 [hep-ph]].

[9] G. Hiller, J. S. Kim and H. Sedello, Phys. Rev. D **80** (2009) 115016 [arXiv:0910.2124 [hep-ph]].

[10] S. Kraml and A. R. Raklev, Phys. Rev. D **73** (2006) 075002 [arXiv:hep-ph/0512284].

[11] M. Carena, A. Freitas and C. E. M. Wagner, JHEP **0810** (2008) 109 [arXiv:0808.2298 [hep-ph]].

[12] S. Bornhauser, M. Drees, S. Grab and J. S. Kim, Phys. Rev. D **83**, 035008 (2011) [arXiv:1011.5508 [hep-ph]].

[13] H. P. Nilles, Phys. Rept. **110** (1984) 1.

[14] M. Dine, W. Fischler and M. Srednicki, Nucl. Phys. B **189** (1981) 575.

[15] M. Dine and W. Fischler, Phys. Lett. B **110** (1982) 227.

[16] M. Dine and A. E. Nelson, Phys. Rev. D **48** (1993) 1277 [arXiv:hep-ph/9303230].

[17] P. Meade, N. Seiberg and D. Shih, Prog. Theor. Phys. Suppl. **177** (2009) 143 [arXiv:0801.3278 [hep-ph]].

[18] M. Buican, P. Meade, N. Seiberg and D. Shih, JHEP **0903** (2009) 016 [arXiv:0812.3668 [hep-ph]].

[19] S. Ambrosanio, G. L. Kane, G. D. Kribs, S. P. Martin and S. Mrenna, Phys. Rev. D **54** (1996) 5395 [arXiv:hep-ph/9605398].

[20] H. Baer, P. G. Mercadante, F. Paige, X. Tata, Y. Wang, Phys. Lett. **B435** (1998) 109-117. [hep-ph/9806290].

[21] S. Shirai, T. T. Yanagida, Phys. Lett. **B680** (2009) 351-354. [arXiv:0905.4034 [hep-ph]].

[22] K. Hamaguchi, M. M. Nojiri, A. de Roeck, JHEP **0703** (2007) 046. [hep-ph/0612060].

[23] J. R. Ellis, A. R. Raklev, O. K. Oye, JHEP **0610** (2006) 061. [hep-ph/0607261].

[24] A. Katz and B. Tweedie, Phys. Rev. D **81** (2010) 035012 [arXiv:0911.4132 [hep-ph]].

[25] Y. Santoso, AIP Conf. Proc. **1200**, 494-497 (2010). [arXiv:0909.4742 [hep-ph]].

[26] P. Meade, M. Reece and D. Shih, JHEP **1005** (2010) 105 [arXiv:0911.4130 [hep-ph]].

[27] Y. Kats and D. Shih, arXiv:1106.0030 [hep-ph].

[28] G. D. Kribs, A. Martin, T. S. Roy, JHEP **0901**, 023 (2009). [arXiv:0807.4936 [hep-ph]].

[29] K. Hamaguchi, S. Shirai, T. T. Yanagida, Phys. Lett. **B663** (2008) 86-94. [arXiv:0712.2462 [hep-ph]].

[30] J. L. Feng, M. Kamionkowski, S. K. Lee, Phys. Rev. **D82** (2010) 015012. [arXiv:1004.4213 [hep-ph]].

[31] P. Meade, M. Reece and D. Shih, JHEP **1010** (2010) 067 [arXiv:1006.4575 [hep-ph]].

[32] G. Aad *et al.* [ATLAS Collaboration], arXiv:1109.2242 [hep-ex].

[33] V. M. Abazov *et al.* [D0 Collaboration], Phys. Rev. Lett. **105** (2010) 221802 [arXiv:1008.2133 [hep-ex]].

[34] G. Aad *et al.* [ATLAS Collaboration], arXiv:1111.4116 [hep-ex].

[35] T. Aaltonen *et al.* [CDF Collaboration], Phys. Rev. Lett. **104** (2010) 011801 [arXiv:0910.3606 [hep-ex]].

[36] G. Aad *et al.* [ATLAS Collaboration], Phys. Rev. Lett. **106** (2011) 121803 [arXiv:1012.4272 [hep-ex]].

[37] S. Chatrchyan *et al.* [CMS Collaboration], [arXiv:1103.0953 [hep-ex]].

[38] L. E. Ibanez, C. Lopez and C. Munoz, Nucl. Phys. B **256** (1985) 218.

[39] M. Drees and K. Hagiwara, Phys. Rev. D **42** (1990) 1709.

[40] M. Vidal, O. Gonzalez [CDF Collaboration], CMS public note 9384 (2009)

[41] U. Sarid and S. D. Thomas, Phys. Rev. Lett. **85** (2000) 1178 [arXiv:hep-ph/9909349].

[42] S. P. Martin and P. Ramond, Phys. Rev. D **48** (1993) 5365 [arXiv:hep-ph/9306314].

[43] S. Dimopoulos, S. D. Thomas and J. D. Wells, Nucl. Phys. B **488** (1997) 39 [hep-ph/9609434].

[44] W. Beenakker, M. Kramer, T. Plehn, M. Spira and P. M. Zerwas, Nucl. Phys. B **515** (1998) 3 [arXiv:hep-ph/9710451].

[45] P. M. Nadolsky, H. -L. Lai, Q. -H. Cao, J. Huston, J. Pumplin, D. Stump, W. -K. Tung, C. -P. Yuan, Phys. Rev. **D78** (2008) 013004. [arXiv:0802.0007 [hep-ph]].

[46] T. Sjostrand, S. Mrenna, P. Z. Skands, JHEP **0605** (2006) 026. [hep-ph/0603175].

[47] S. Ovyn, X. Rouby, V. Lemaitre, [arXiv:0903.2225 [hep-ph]].

[48] T. Junk, Nucl. Instrum. Meth. **A434** (1999) 435-443. [hep-ex/9902006].

[49] A. L. Read, J. Phys. GG **28** (2002) 2693.

[50] J. Conway [CDF Collaboration], Proceedings of the Workshop on Confidence Limits, Geneva, Switzerland, 17-18 Jan 2000

[51] G. Aad *et al.* [Atlas Collaboration], Phys. Rev. D **83** (2011) 052005 [arXiv:1012.4389 [hep-ex]].

[52] G. Aad *et al.* [Atlas Collaboration], ATLAS-CONF-2010-005 (2010), `http://cdsweb.cern.ch/record/1273197`

[53] G. Aad *et al.* [The ATLAS Collaboration], arXiv:0901.0512 [hep-ex].

[54] S. Chatrchyan *et al.* [The CMS Collaboration], CMS-PAS-EXO-11-067 (2011), `http://cdsweb.cern.ch/record/1394286/`

[55] R. Brun, F. Rademakers, Nucl. Instrum. Meth. **A389** (1997) 81-86.

[56] We modify `Delphes` slightly to simulate a DØ-like calorimeter with > 40 segments in η direction and flag gravitinos as undetectable particles.

[57] We use the implementation in the `TLimit` class of `ROOT 5.28.00b`[55].

[58] We also performed the calculation for the $36\,\mathrm{pb}^{-1}$ CMS $\gamma\gamma\not{E}_T$ results [37]. These impose a weaker bound on $\mathcal{B}(\tilde{t}_1 \to c\tilde{\chi}_1^0)$ than the $6.3\,\mathrm{fb}^{-1}$ DØ data [33].

[59] The ratio of the energy deposits in 3×7 and 7×7 cells $(\eta\times\phi)$ in the electromagnetic calorimeter contributing to the photon cluster, and the shower's lateral width.